Journal of Structural Geology 32 (2010) 886–899

Contents lists available at ScienceDirect

Journal of Structural Geology

journal homepage: www.elsevier.com/locate/jsg

Kinematic analysis of a transtensional fault system: The Atuel depocenter of the Neuquén basin, southern Central Andes, Argentina

Florencia Bechis [a,*], Laura Giambiagi [b], Víctor García [c], Silvia Lanés [d], Ernesto Cristallini [c], Maisa Tunik [e]

[a] CONICET – IIDyPCA, Universidad Nacional de Río Negro (UNRN), Sarmiento Inferior 3974, CP 8400, San Carlos de Bariloche, Argentina
[b] CONICET – IANIGLA, CCT Mendoza, CC 330, CP 5500, Mendoza, Argentina
[c] CONICET – Laboratorio de Modelado Geológico, FCEN, UBA, Pabellón 2, Ciudad Universitaria, CP 1428, Buenos Aires, Argentina
[d] E505 East Tower, Knightsbridge, Esplanade Road, Century City, 7441, Cape Town, South Africa
[e] CONICET – CIMAR, UNCOMA, Av. Buenos Aires 1300, CP 8300, Neuquén, Argentina

ARTICLE INFO

Article history:
Received 4 December 2009
Received in revised form
16 March 2010
Accepted 19 March 2010
Available online 7 April 2010

Keywords:
Oblique rift
Transtension
Kinematic analysis
Neuquén basin
Central Andes

ABSTRACT

The Atuel depocenter of the Neuquén basin originated as an Upper Triassic to Lower Jurassic rift system, later inverted during the Andean contractional deformation. In order to study the extensional architecture and the kinematic evolution of this depocenter, we collected a large amount of field and subsurface data, consisting of slip data from outcrop-scale normal faults, thickness and facies distribution within the synrift deposits, and structural data from angular and progressive unconformities. The Atuel depocenter has a NNW trend, showing a bimodal distribution of NNW and WNW major faults (first and second order faults). On the other hand, from kinematic indicators measured on outcrop-scale faults (third and fourth order faults), we found a mean NE internal extension direction, which is oblique to the general trend of the sub-basin. Taking these particular characteristics into account, we interpreted the Atuel depocenter as an oblique rift system. We evaluated two mechanisms in order to explain the development of this transtensional system: 1) reactivation of upper-crustal NNW-oriented Paleozoic shear zones, and 2) oblique stretching of a previous NNW-oriented lithospheric weakness zone.

1. Introduction

The Neuquén basin began as a rift basin during Late Triassic to Early Jurassic times (Uliana et al., 1989; Vergani et al., 1995; Franzese and Spalletti, 2001). The early synrift sequences are restricted to isolated depocenters limited by normal faults, with variable orientations according to their geographical position within the basin (Vergani et al., 1995). Mosquera and Ramos (2006) interpreted this variability as being related to a strong control of the basement structural grain. According to several authors (Ramos, 2010; and references therein), the regional extensional regime continued during Middle Jurassic to Early Cretaceous times, related to a negative roll-back of the Pacific subduction trench line. By the end of the Early Cretaceous period, the opening of the South Atlantic Ocean and the consequent separation of South America from Africa marked the start of contractional deformation and basin inversion in the southern Central Andes (Cobbold and Rosello, 2003; Zamora Valcarce et al., 2006; Somoza and Zaffarana, 2008).

The Neuquén basin has two well defined sectors: the Neuquén embayment, and the Andean sector (Fig. 1). The main difference between them is that the embayment has not been affected by the Andean contractional deformation, due to its foreland position. We focused our research on the Atuel depocenter, situated in the northern Andean sector (Fig. 1). Its Late Triassic to Early Jurassic sedimentary infill records the first stages of the basin opening as a rift system (Manceda and Figueroa, 1995; Lanés, 2002, 2005; Lanés et al., 2008; Giambiagi et al., 2005, 2008a; Bechis et al., 2009; Tunik et al., 2008; Bechis, 2009). In Neogene times, the Andean orogeny deformed and uplifted the depocenter infill, favoring the exhumation of the synrift deposits and their exposure in the northern sector of the Malargüe fold and thrust belt (Fig. 1b; Giambiagi et al., 2008b; Bechis et al., 2008).

In this paper, we analyze the extensional architecture and the kinematic evolution of the Atuel depocenter from the integration of multi-scale structural data. Faults of different scales can give different types of information. Major faults control the location of the main depocenters and the distribution of the sedimentary environments, but they can be the result of previous anisotropies reactivation; undergo a progressive syntectonic rotation along

* Corresponding author. Fax: +54 2944 441809.
E-mail addresses: florbechis@gmail.com (F. Bechis), lgiambia@lab.cricyt.edu.ar (L. Giambiagi), victorg@gl.fcen.uba.ar (V. García), lucero_sil@yahoo.com.ar (S. Lanés), ernesto@gl.fcen.uba.ar (E. Cristallini), mtunik@uncoma.edu.ar (M. Tunik).

0191-8141/$ – see front matter © 2010 Elsevier Ltd. All rights reserved.
doi:10.1016/j.jsg.2010.03.009

their activity history; or change their sense of slip through time. In addition, subsequent tectonic phases often reactivate or cover them, making recognizing and studying them difficult. On the other hand, small-scale faults often escape subsequent reactivation and are generally abundant and well exposed. Moreover, strain or stress inversion methods based on the analysis of slip data from small-scale faults can give key information about the kinematics and dynamics of previous tectonic events (Angelier, 1984; Marrett and Allmendinger, 1990; Twiss and Unruh, 1998; Gapais et al., 2000).

In our study, we integrate new field data (from geological and structural mapping), and previous stratigraphic, sedimentological and structural data (Manceda and Figueroa, 1995; Lanés, 2002, 2005; Lanés et al., 2008; Giambiagi et al., 2005, 2008a, 2008b; Bechis et al., 2008, 2009; Tunik et al., 2008; Bechis, 2009), as well as seismic and well-log data acquired by the oil industry. We present a kinematic model for the evolution of the Atuel depocenter as an oblique rift system, taking into account data from minor and major normal faults. We also evaluate the possible factors controlling the transtensional deformation of the sub-basin, such as reactivation of previous anisotropies or lithospheric weakness, and the direction of regional extension.

2. Stratigraphic setting

The structural basement of the Neuquén basin crops out in the northeastern sector of the study area, at the southern end of the Frontal Cordillera (Figs. 1 and 2). In this sector, the basement is composed of Paleozoic metasedimentary rocks, Carboniferous plutons, and widespread outcrops of the Choiyoi Group, a Permian to Triassic volcanic and plutonic complex (Volkheimer, 1978; Llambías et al., 1993; Sruoga et al., 2005).

The Upper Triassic to Lower Jurassic infill of the Atuel depocenter consists of siliciclastic marine and continental sedimentary rocks, grouped in the Arroyo Malo, El Freno, Puesto Araya and Tres Esquinas Formations (Figs. 2 and 3; Reijenstein, 1967; Volkheimer, 1978; Riccardi et al., 1991, 1997; Lanés, 2002, 2005; Lanés et al., 2008; Spalletti et al., 2007). Lanés (2002, 2005) and Lanés et al. (2008) used the accommodation versus sedimentary supply ratio to identify two stages of differing tectonic behavior (Fig. 3). The first one corresponds to the synrift stage, from Rhaetian to late Early Sinemurian times, showing greater accommodation than sedimentary supply (Lanés, 2002, 2005). This period was characterized by deposition of slope-type fan deltas in the western sector, while in the eastern sector a coeval braided fluvial system developed (Fig. 3; Lanés, 2002, 2005; Lanés et al., 2008; Tunik et al., 2008). A paleogeography dominated by active normal faulting controlled the marked lateral variations of the depositional systems during this stage. It is important to note that the base of the synrift units is always below the present exposure level, making it impossible to observe the contact between the structural basement and the sedimentary infill of the Atuel depocenter. The second stage, from late Early Sinemurian to Toarcian times, shows varying accommodation. During the late Early Sinemurian period, accommodation was outpaced by sedimentary supply, marking the start of the sag phase. An intermediate-type fan delta prograded over the slope-type fan deltas in the western sector, while in the eastern sector the fluvial systems increased their lateral migration (Lanés, 2002, 2005; Lanés et al., 2008). Later, during late Early Sinemurian to Toarcian times accommodation exceeded the supply, allowing transgression of a marine shelf and a marked increase in the marine depositional area (Fig. 3).

In the study area, the Middle Jurassic to Paleogene infill of the Neuquén basin consists of a thick pile of evaporitic, carbonatic and clastic marine and continental sedimentary rocks, assigned to the Lotena, Mendoza, Bajada del Agrio, Neuquén and Malargüe Groups (Fig. 2; Legarreta et al., 1993; Gulisano and Gutiérrez Pleimling, 1994; Legarreta and Uliana, 1996).

Cenozoic magmatic rocks correspond to Miocene to Quaternary andesitic to basaltic volcanic and subvolcanic rocks (Fig. 2; Volkheimer, 1978; Baldauf, 1997; Nullo et al., 2002; Sruoga et al., 2005; Giambiagi et al., 2008b). Thick clastic and volcaniclastic deposits crop out in the eastern sector, representing the Miocene to Pleistocene synorogenic infill of the Andean foreland basin (Fig. 2; Yrigoyen, 1993; Baldauf, 1997; Combina and Nullo, 2000; Giambiagi et al., 2008b).

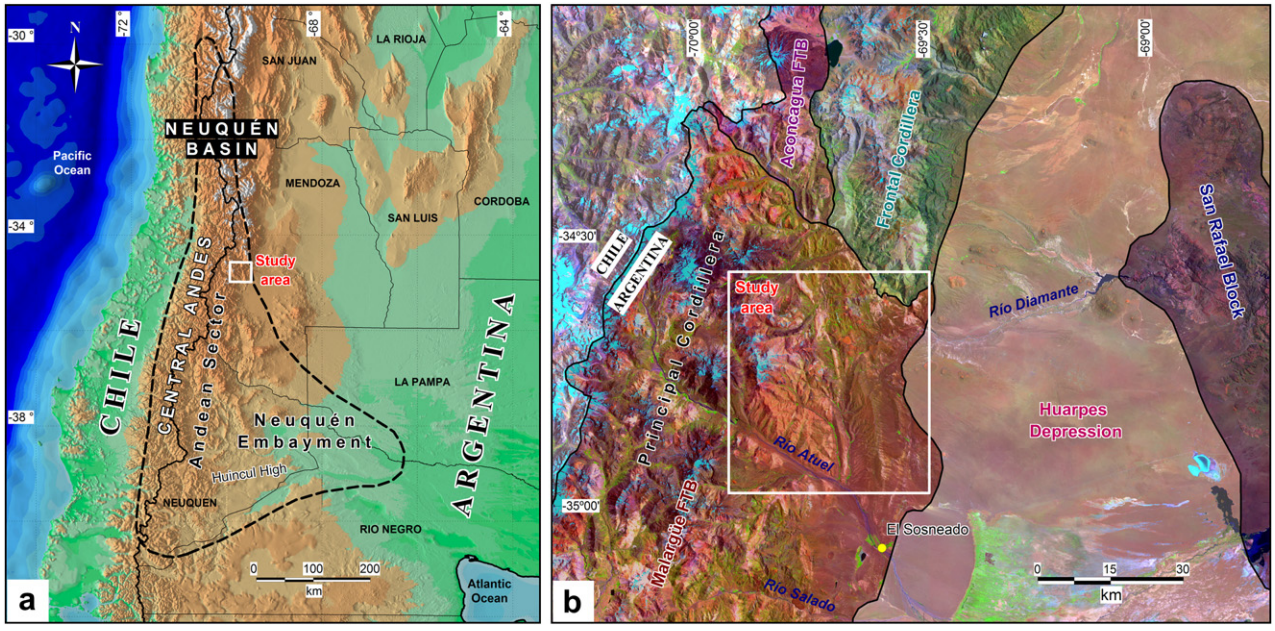

Fig. 1. a) Regional location map showing the Neuquén basin limits and the Atuel depocenter location, in the northern Andean sector of the basin. b) Landsat satellite image showing the study area in the context of the local morphostructural units. FTB: fold and thrust belt.

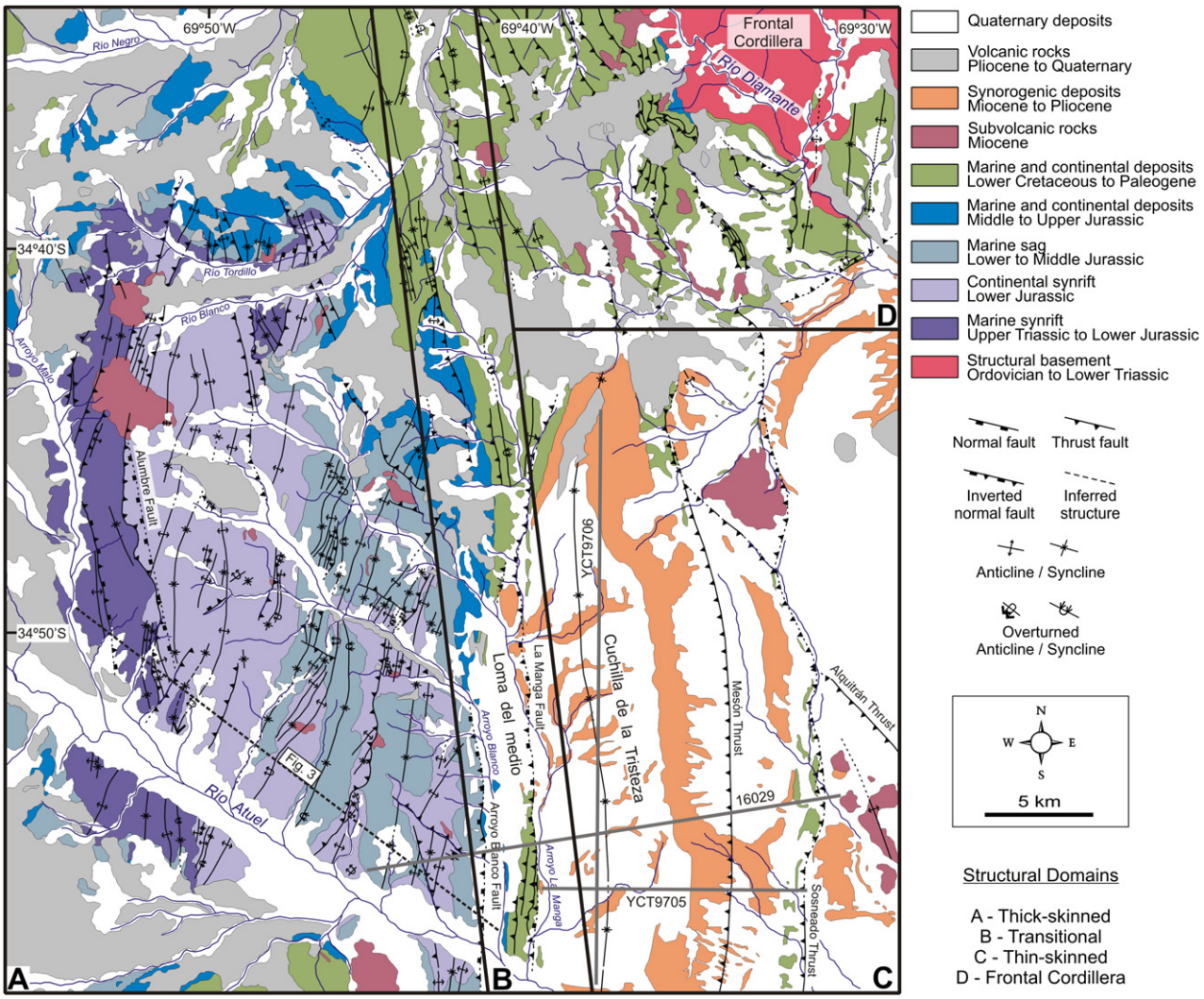

Fig. 2. Geological and structural map of the study area (modified from Giambiagi et al., 2008b; see references therein).

3. The Malargüe fold and thrust belt

The Malargüe fold and thrust belt has a regional thick-skinned structural style, with local development of triangular zones and shallow thin-skinned areas (Kozlowski et al., 1993). Its northern sector is characterized by a western thick-skinned zone, with the basement involved in the deformation; and an eastern thin-skinned sector, with shallow low-angle thrusts developed within the Mesozoic and Cenozoic sedimentary cover. The limit between these two areas of contrasting structural style is marked by a regional lineament of NNW trend (Fig. 2, domain B), with a strong deformation characterized by a stack of basement sheets bordered by east-vergent high-angle reverse faults (Fig. 4; Kozlowski, 1984; Manceda and Figueroa, 1995; Dimieri et al., 2005; Giambiagi et al., 2008b).

In the western thick-skinned sector, the synrift and sag deposits of the Atuel depocenter crop out, showing an intense contractional deformation (Fig. 2, domain A). Most folds and reverse faults show a NNE orientation, but NNW trends are locally observed. Contractional structures are segmented by WNW lineaments that acted as transfer zones during the Andean deformation. The main detachment level of the western sector is located within the basement, whilst secondary detachments developed in the Lower Jurassic units (Kozlowski, 1984; Fortunatti and Dimieri, 2006; Giambiagi et al., 2008b).

In the eastern thin-skinned sector, Cretaceous to Quaternary strata are deformed by east-verging low-angle thrust faults, showing N–NNW trends (Fig. 2, domain C; Kozlowski et al., 1993). In this area, Neogene synorogenic deposits crop out, showing angular and progressive unconformities that mark the contractional deformation pulses (Kozlowski, 1984; Combina and Nullo, 2000; Giambiagi et al., 2008b). The main detachment level is located within Cretaceous shaley and evaporitic sequences (Fig. 4; Kozlowski, 1984).

In the northeastern sector of the study area a basement block represents the Frontal Cordillera southern end (Fig. 2, domain D). This block corresponds to an asymmetric anticline, limited to the east by an important inverse fault of eastward vergence and to the west by minor backthrusts (Kozlowski, 1984; Turienzo and Dimieri, 2005).

4. Extensional arquitecture of the Atuel depocenter

We carried out detailed mapping of the Upper Triassic to Lower Jurassic units in order to identify the Mesozoic extensional structures. We classified the observed and interpreted faults in four

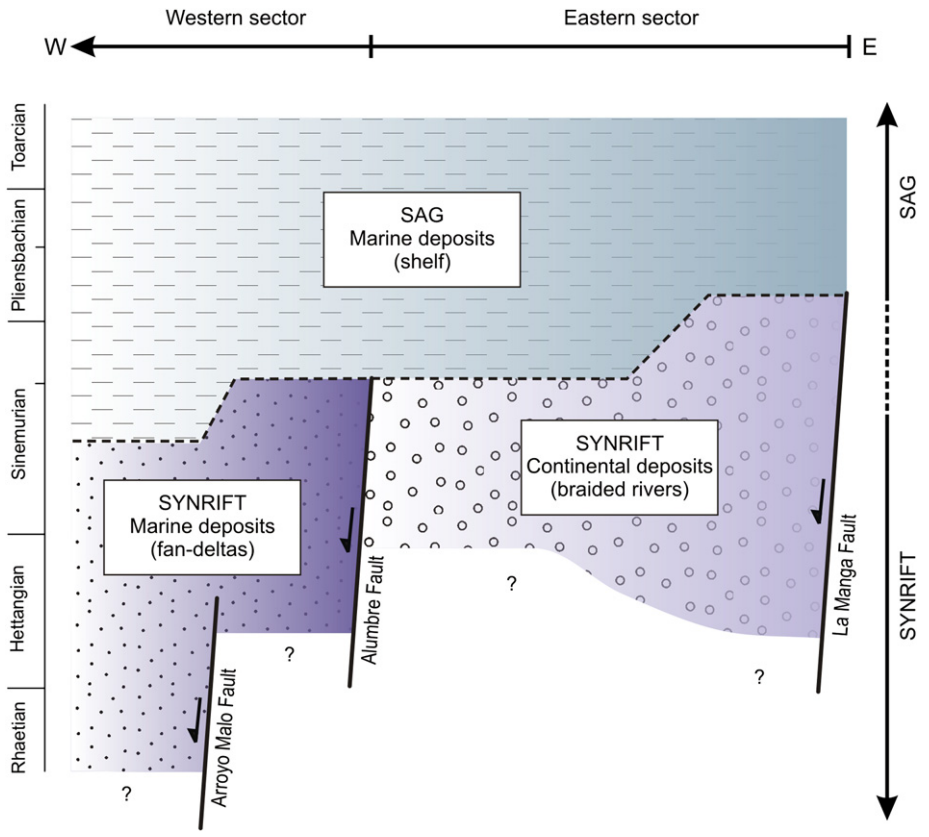

Fig. 3. Simplified section showing the synrift and sag units that constitute the Upper Triassic to Lower Jurassic infill of the Atuel depocenter (modified from Lanés et al., 2008). Note that the base of the synrift units is always below the exposure level. See orientation of the section in Fig. 2. The section is not to scale.

orders according to their dimensions and their control over the subsidence and distribution of the sedimentary environments during the synrift phase (Table 1).

4.1. First and second order faults

Most of the first and second order Mesozoic normal faults have been inverted or cut by the Andean contractional structures, or covered by younger deposits. In order to identify the trend and location of these major normal faults we integrated different lines of evidence:

- Controls of the previous extensional structures over the contractional Andean deformation: sharp changes in the structural style, anomalies in the orientation of structures, location of transfer zones, and the evolution of the fold and thrust belt (Fig. 5).
- Location and sense of tilting of syntectonic angular and progressive unconformities affecting the Upper Triassic to Lower Jurassic deposits (Fig. 6).
- Evidence of active deformation during the sedimentation: variations in synrift thickness across structures, clastic dikes, unconformities cutting the faults, small-scale faults (Fig. 7), synsedimentary folds or slumps.
- Lateral facies and thickness variations of the synrift deposits (Figs. 3, 5 and 6).

From the integration of these data, we noted that the development of two first order faults of NNW trend controlled the general orientation of the Atuel depocenter. These are the La Manga and Alumbre faults, marked by the superficial and subsoil distribution of the synrift deposits (Figs. 3 and 5; Giambiagi et al., 2008a). These major structures controlled most of the basin subsidence, the distribution of the sedimentary environments and the drainage patterns during the synrift stage (Lanés, 2002, 2005; Lanés et al., 2008). While fluvial sediments characterize the synrift infill in the hanging-wall of the La Manga fault, coetaneous deposits to the west of the Alumbre fault were deposited in a marine fan-deltaic environment (Figs. 3 and 5; Lanés, 2002, 2005; Tunik et al., 2008).

The La Manga fault was the eastern border of the Atuel depocenter, which was strongly inverted during the Andean deformation (Figs. 2 and 4c; Giambiagi et al., 2008b). This fault coincides with the NNW lineament that separates the western thick-skinned sector from the eastern area of shallow deformation in the fold and thrust belt (Fig. 2). To the east of La Manga fault, there is no record of Upper Triassic to Lower Jurassic synrift deposits either in outcrops or in wells, while more than 1500 m of continental synrift deposits are registered in its hanging-wall (Figs. 3–5).

The NNW-trending Alumbre fault maintained a nearly fixed position of the coastal line from Hettangian to Early Sinemurian times, restricting the marine sedimentation to the western sector of the Atuel depocenter. Fan-deltaic deposits in the hanging-wall of the Alumbre fault show a marked cuneiform geometry, with strata thickening towards the structure. The synrift sequence shows angular and progressive unconformities indicating a progressive eastward tilting of its hanging-wall (Fig. 6). In one of the examples, the progressive unconformities are related to a syncline structure, indicating that folding was active during synrift sedimentation (Fig. 6d). These observations enable us to interpret this syncline as an extensional fault propagation fold (Hardy and McClay, 1999).

In the Atuel depocenter, second order faults have a NNW and WNW bimodal distribution (Figs. 5 and 6). These faults controlled

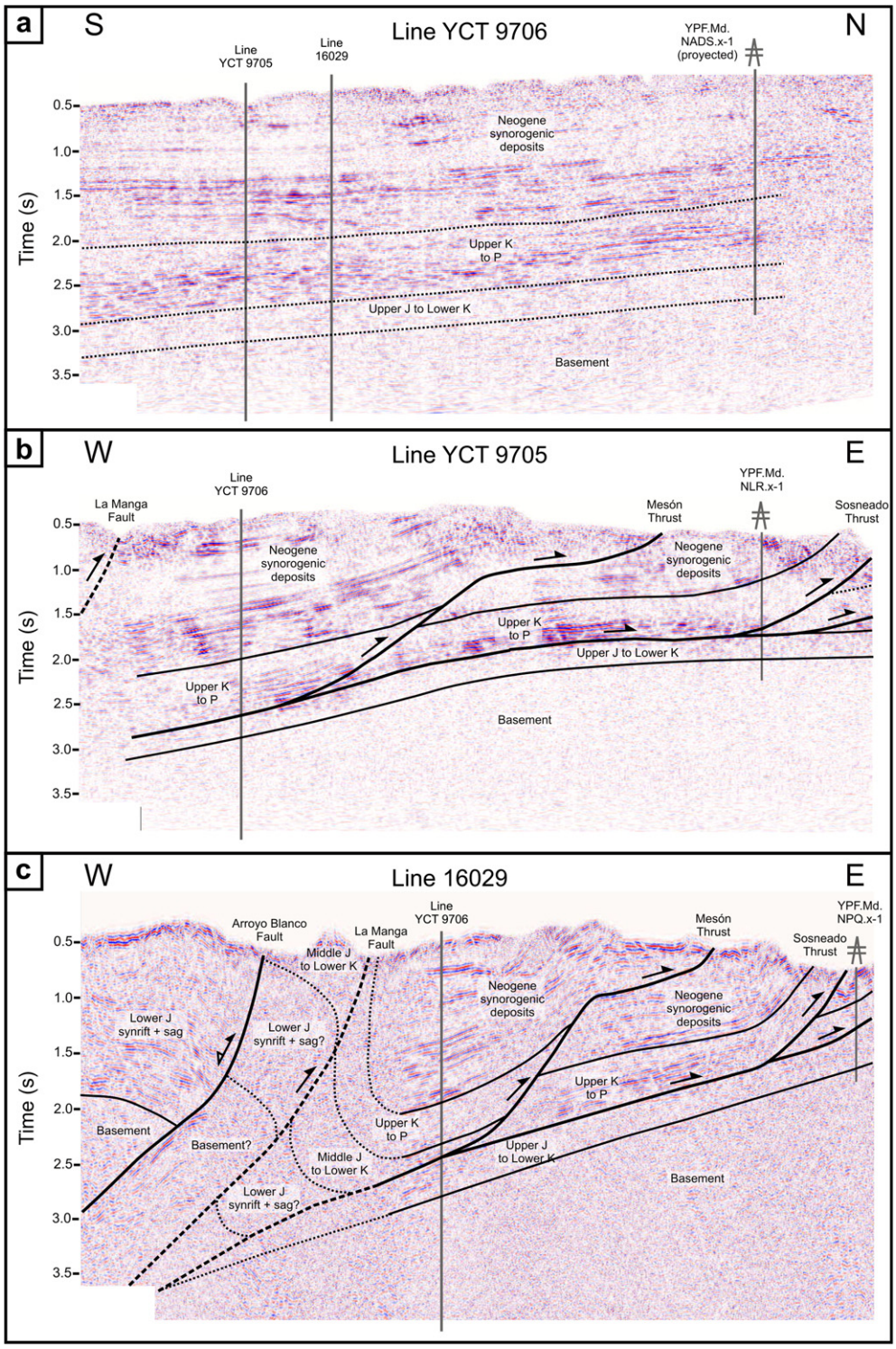

Fig. 4. Interpretation of seismic lines, showing the structural styles and the lack of Upper Triassic to Middle Jurassic units in the eastern sector of the fold and thrust belt (Fig. 4c modified from Giambiagi et al., 2008b). Note the high thickness of synrift deposits to the west of La Manga fault. See Fig. 2 for location. J: Jurassic, K: Cretaceous, P: Paleogene.

minor facies and lateral environmental variations of the synrift deposits, as in the case of the Atuel fault. According to Giambiagi et al. (2008a), sedimentary structures indicate a shallower fan-deltaic environment to the south of this fault, compared to the deep fan-deltaic setting described by Lanés (2002, 2005) to the north. Second order faults also generated relatively high gradient slopes where synsedimentary deformation structures developed. For example, Lanés (2002) suggested that the Arroyo Malo fault explained the presence of abundant slumps within the slope-type fan-deltaic sequence of Upper Triassic age. Second order faults also controlled the development of angular and progressive unconformities within the synrift strata (Fig. 6). During the Andean deformation, WNW second order faults acted as transfer zones, while some of the NNW normal faults were inverted, producing

Table 1
Classification of faults in four orders, according to their main characteristics.

Fault order	Length	Throw	Andean reactivation	Controls on depositional systems
First	>10 km	>1 km	Common	Distribution of the depositional environments, generation of accommodation space
Second	5–10 km	50–1000 m	Common	Minor variations in the depositional environments, control on drainage network
Third	<5 km	1–50 m	Occasional	Local deformation in the hanging-wall of major faults
Fourth	?	<1 m	Rare	Minor local deformation in the hanging-wall of major faults

curvatures and changes in the strike of the Neogene thrusts (Figs. 2 and 5).

4.2. Third and fourth order faults

We identified more than 300 outcrop-scale normal faults affecting the synrift strata, corresponding to third and fourth order faults (Fig. 7). Third order faults have several meters of displacement, while fourth order faults show less than 1 m of displacement. We paid particular attention to the identification of characteristics that confirmed the Upper Triassic to Lower Jurassic age of the measured faults, such as the thickening of the strata in their hanging-wall, the presence of related progressive and angular unconformities, or fault fossilization by younger synrift strata.

While fourth order faults in general are well preserved, some of the third order faults show two sets of striations or have reactivated during the Andean contraction (Giambiagi et al., 2005). We

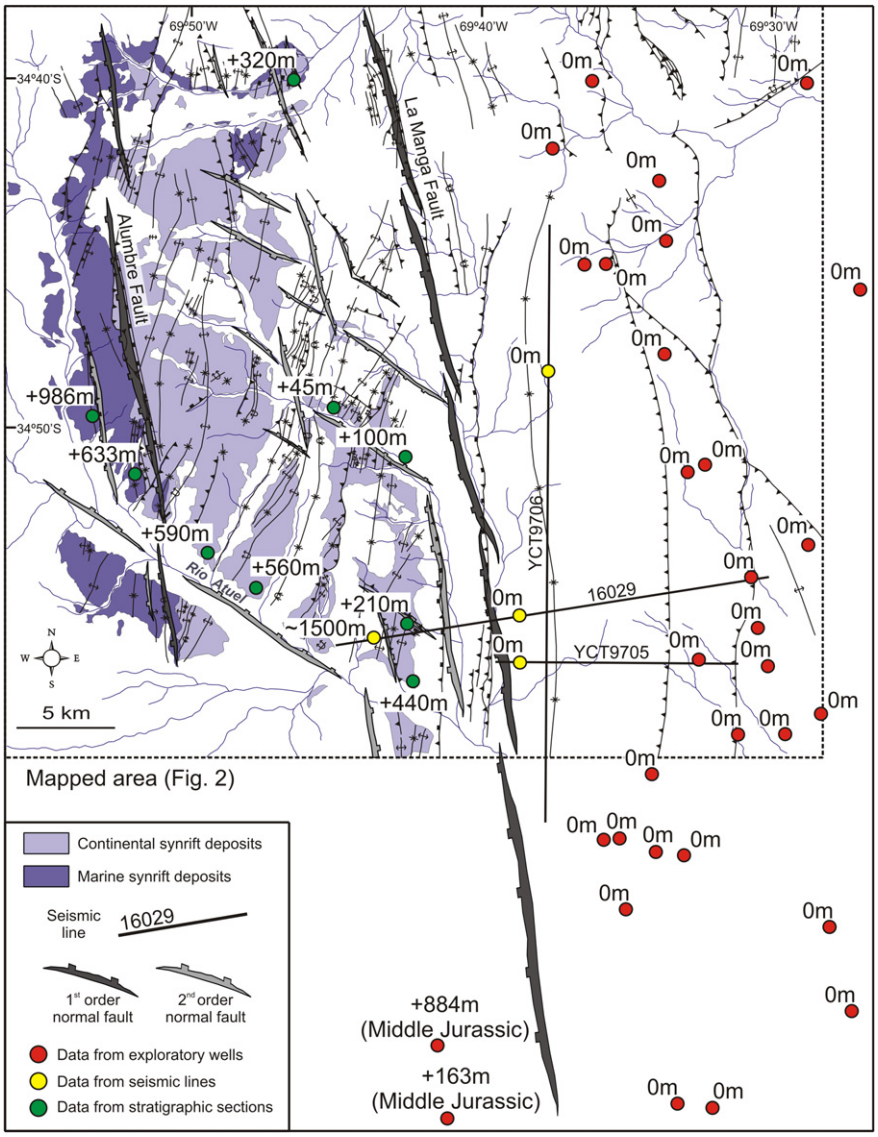

Fig. 5. Map showing the superficial and sub-surface thickness distribution of the synrift units of the Atuel depocenter. Neogene contractional structures are also represented in order to show their relationship with respect to the interpreted first and second order normal faults. Thickness values obtained from field data of stratigraphic sections (Lanés, 2002, 2005; Giambiagi et al., 2005; Lanés et al., 2008), from sub-surface data of exploratory wells, and from lateral interpolations using seismic lines (Fig. 4). In wells where the synrift is absent (0m of thickness), Upper Jurassic units lie directly on top of the structural basement. In the southern central sector of the map, two wells cross a thick Middle Jurassic section, not reaching its base.

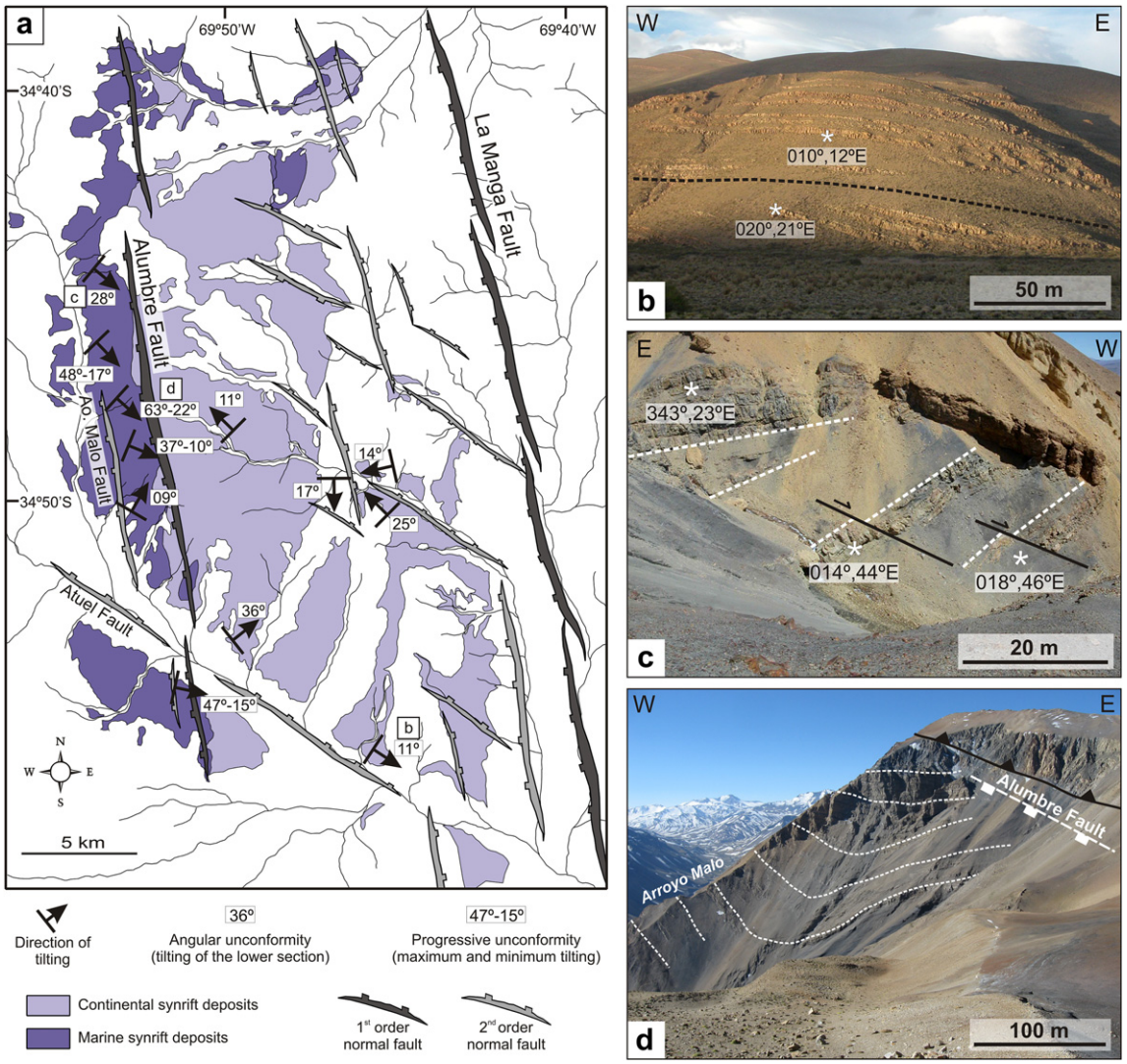

Fig. 6. a) Map showing tilted strata from angular and progressive unconformities. Angular values correspond to the lower section tilting, in the case of angular unconformities, or the maximum and minimum tilting from base to top, in the case of progressive unconformities (data restored to their original position prior to the Andean folding using the software StereoWin®; Allmendinger, 2002). b) Angular unconformity affecting the fluvial synrift deposits, in the hanging-wall of the La Manga fault. c) Small-scale faults and related unconformities affecting the fan-deltaic synrift deposits, in the hanging-wall of the Alumbre fault. d) Growth syncline interpreted as a fault propagation fold related to the Alumbre fault. See location of figures b–d in the map.

identified a large number of minor faults in the synrift fan-deltaic deposits of the western sector of the Atuel depocenter, while the conglomerate nature and greater thickness of the fluvial synrift beds of the eastern sector made it more difficult to recognize small-scale faults.

Outcrop-scale normal faults show a variable trend, with a concentration of data in a range between WNW and NNE orientations. In the case of the third order faults, we found three well defined groups: NNW, WNW and NNE (Fig. 8). Fourth order faults show greater dispersion, but in general the trend distribution is similar to the orientation of the major faults (Fig. 8).

5. Kinematic data set

We measured fault-slip data in more than 250 third and fourth order normal faults, grouped in 12 stations widely distributed within the Atuel depocenter (Table 2, Fig. 9). We classified the stations according to the age of the synrift deposits, including strata of Upper Triassic to Hettangian age in the early synrift, and sediments of Lower Sinemurian age in the late synrift. We measured direction and sense of slip using kinematic indicators, according to the criteria proposed by Petit (1987). In most cases, kinematic indicators corresponded to mechanical striations and secondary fractures (mainly Riedel-type fractures; Fig. 7). We observed a large number of faults without development of striae, and we tentatively relate this absence to a low consolidation of the sediments during the deformation.

We restored the obtained kinematic data to their original position, previous to the Andean contractional deformation, by rotating local bedding back to a horizontal position around its strike azimuth. We processed the restored data using the graphic method based on Bingham distribution statistics (see Marrett and Allmendinger, 1990 for methodological details), in order to estimate the orientation of the main axes of the strain ellipsoid ($\lambda 1$, $\lambda 2$ and $\lambda 3$) for each measurement station (using the software FaultKinWin®, Allmendinger, 2001).

At all stations, the intermediate and major axes of the strain ellipsoid ($\lambda 2$ and $\lambda 1$) show a sub-horizontal position, indicating an

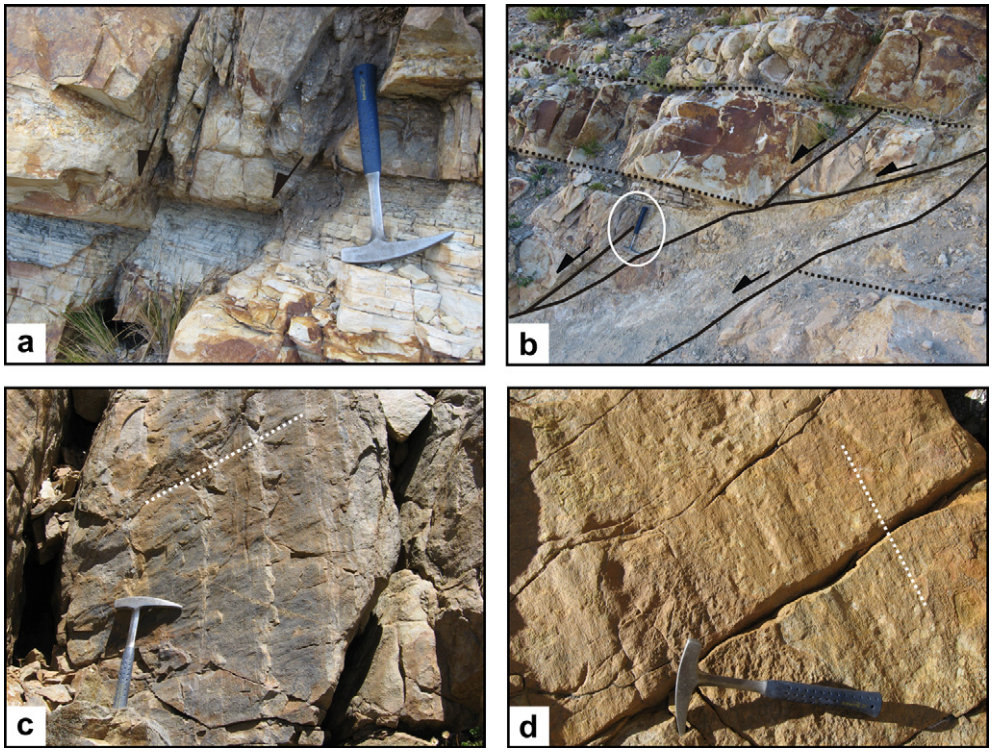

Fig. 7. Photographs showing examples of fourth order (a) and third order (b) normal faults. c and d) Examples of fault planes showing mechanical striations and related secondary fractures, used as kinematic indicators.

extensional tectonic regime (subvertical $\lambda 3$; Table 2). In most stations, normal faults show a main extension direction ($\lambda 1$) between NNE and ENE orientations. Using these data we calculated a mean $\lambda 1$ oriented to the NE (mean $\lambda 1$ = Az 047°; Fig. 9). Third to fourth order faults can be separated in three groups according to their kinematic characteristics and their geographic distribution (Fig. 10).

5.1. Faults indicating a NNE to NE extension, inner sector of the Atuel depocenter

Third to fourth order faults observed in the inner sector of the Atuel depocenter show a wide dispersion of trends ranging from WNW to NNW, and they indicate NNE to NE extension directions (Figs. 9 and 10). We calculated an Az 040° direction for the internal extension of the depocenter (Fig. 10).

Some of the stations where we found NE–NNE extension directions are located in the hanging-wall of the Alumbre fault (Figs. 9 and 11). Taking into account the obliquity between the extension directions and the NNW trend of the fault, we interpret an oblique-normal slip for the Alumbre fault, with a left-lateral component. We infer a local clockwise rotation of its hanging-wall, based on evidence of the change between the extension directions obtained from early and late synrift strata (Fig. 11). In their palaeomagnetic studies, Iglesia Llanos et al. (2006) and Iglesia Llanos (2008) did not find large tectonic block rotations around vertical axes within the Atuel depocenter. Thus, the clockwise rotation related to the Alumbre fault represents a local effect.

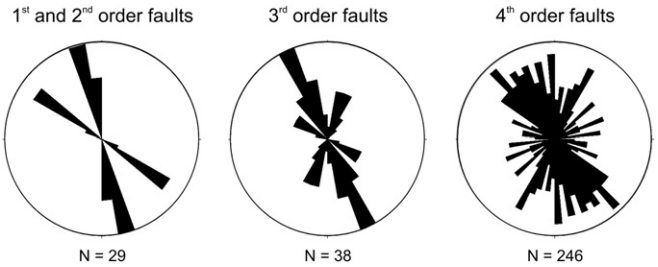

Fig. 8. Rose diagrams showing the fault trend distribution, according to their order. Diagrams made using the StereoWin® program (Allmendinger, 2002).

5.2. Faults indicating an ENE extension, eastern border of the Atuel depocenter

We measured small-scale faults with trends ranging from NNW to NNE in the southeastern sector of the depocenter, indicating an ENE extension oriented to the Az 077° (Figs. 9 and 10). The obtained direction is similar to the ENE extension (Az 062°) interpreted by Giambiagi et al. (2005) in the northeastern sector of the Atuel depocenter, based on the orientation and slip of third order faults. Both the faults observed by Giambiagi et al. (2005) in the northeastern sector and the faults we measured affect the upper section of the continental synrift deposits and the lower section of the marine shelf deposits, of Late Sinemurian to Early Pliensbachian age, coinciding with the end of the synrift period and the start of the sag phase (Lanés, 2002, 2005; Lanés et al., 2008).

Stations where we found an ENE extension are located in the hanging-wall of the La Manga fault, showing a maximum extension direction nearly orthogonal to its trend during the latest synrift period (Figs. 9 and 10). We interpret a predominantly normal slip for the La Manga fault, at least during the late synrift stage.

5.3. Faults indicating a NW extension (related to Andean deformation?)

At stations 4 and 7, we measured NE-oriented normal faults indicating a NW-directed extension (Figs. 9, 10 and 12). These

Table 2
Kinematic data from measurement stations. N: number of data. $\lambda 1$, $\lambda 2$ y $\lambda 3$: major, intermediate and minor axes of the strain ellipsoid. Indicated values correspond to the strike and dip of each axe, using the right hand convention.

Station	Location		Strata age	N	Axes of the strain ellipsoid					
	Latitude	Longitude			$\lambda 1$		$\lambda 2$		$\lambda 3$	
1	−34.792	−69.890	Triassic to Middle Hettangian	12	238.0	4.8	147.7	3.9	18.8	83.8
2	−34.824	−69.877	Pre-Lower Sinemurian	16	241.3	23.5	151.2	0.3	60.5	66.5
3	−34.825	−69.875	Lower Sinemurian	17	29.5	9.0	297.9	10.3	159.9	76.2
4a	−34.888	−69.879	Hettangian?	14	48.4	3.8	317.7	10.1	158.7	79.2
4b	−34.888	−69.879	Hettangian?	7	322.9	2.9	232.2	14.2	64.2	75.5
5	−34.903	−69.854	Pre-Upper Sinemurian	10	39.3	1.2	129.3	3.4	289.9	86.3
7	−34.920	−69.821	Pre-Upper Sinemurian	49	327.1	5.2	236.5	6.0	97.7	82.0
8	−34.892	−69.794	Pre-Upper Sinemurian	7	40.1	20.5	136.0	15.6	260.5	63.8
9	−34.947	−69.767	Pre-Lower Pliensbachian?	50	264.2	11.6	356.7	11.9	131.0	73.3
10	−34.954	−69.732	Lower Pliensbachian	44	76.3	24.5	344.3	4.4	244.7	65.0
11	−34.759	−69.888	Lower Sinemurian?	4	13.7	27.4	283.6	0.1	193.4	62.6
12	−34.844	−69.880	Lower Sinemurian?	16	15.6	2.1	285.6	0.5	181.6	87.8
				246						

Bold value represents the sum of number of data of all stations.

stations are located near the hinge of two major NE-trending Andean anticlines, and the normal faults present a similar NE trend, indicating a NW extension direction nearly orthogonal to the axes of the folds (Fig. 12). In addition, faults indicating a NE-directed extension show more consistent kinematics after restoring them to the position they had prior to the Andean deformation, while the ones that indicate a NW-directed extension present a better grouping before the unfolding (Fig. 12). Taking into account all these characteristics, we interpret that the NW extension direction is probably the result of the bending of strata during the Andean folding.

6. Kinematic model

The Alumbre and La Manga major faults had a significant slip (>1 km) and they controlled the general NNW orientation of the Atuel depocenter. Taking into account the obliquity between the NNW extended area and the average NE extension obtained from kinematic data (mean $\lambda 1$ = Az 047°), we interpret that the depocenter evolved as an oblique rift system (Fig. 13). The large slip of these faults might have been responsible for several characteristics that differentiate the Atuel depocenter from other depocenters in

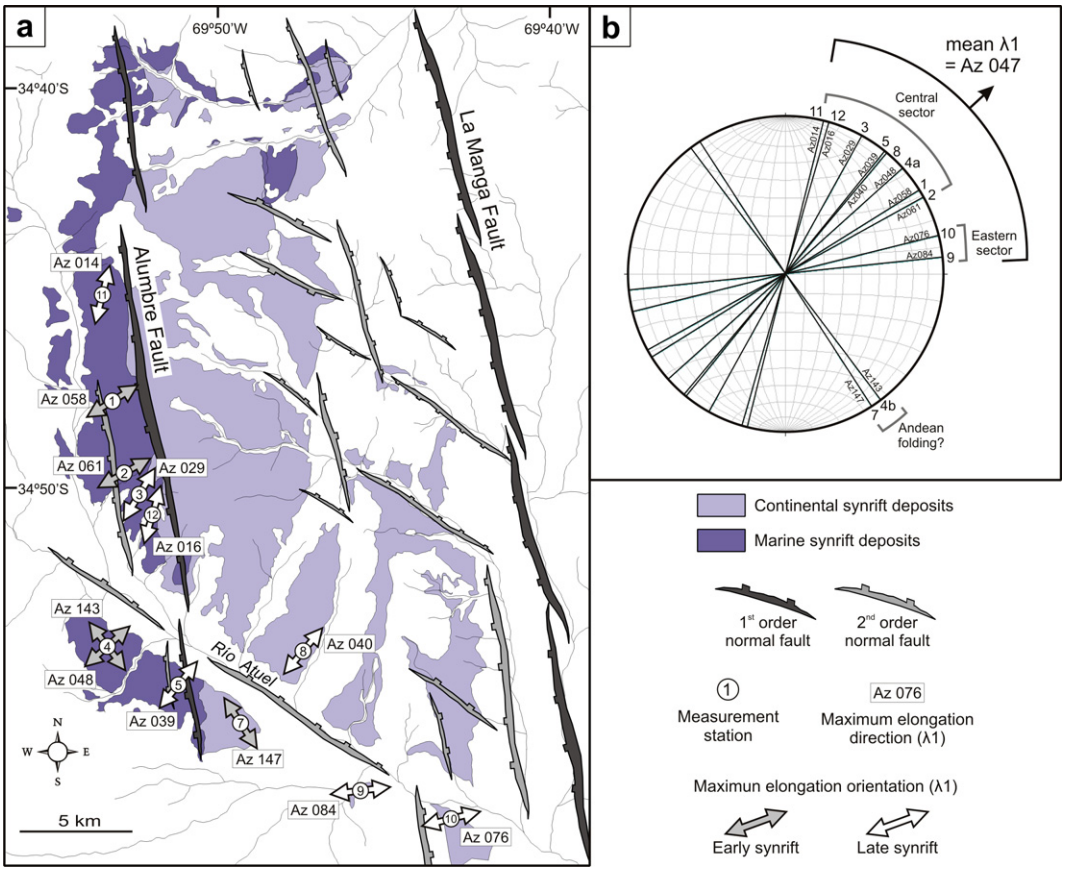

Fig. 9. a) Map showing the location of the stations with measured kinematic data from outcrop-scale faults. The double arrows indicate the orientation of the major axe of the obtained strain ellipsoid ($\lambda 1$). In every case, the minor axe ($\lambda 3$) is subvertical. Early synrift data correspond to faults affecting Upper Triassic to Hettangian deposits, while late synrift data were measured in Lower Sinemurian sediments. b) Orientation of the maximum elongation obtained ($\lambda 1$) for all the measurement stations. See location of each station in the map.

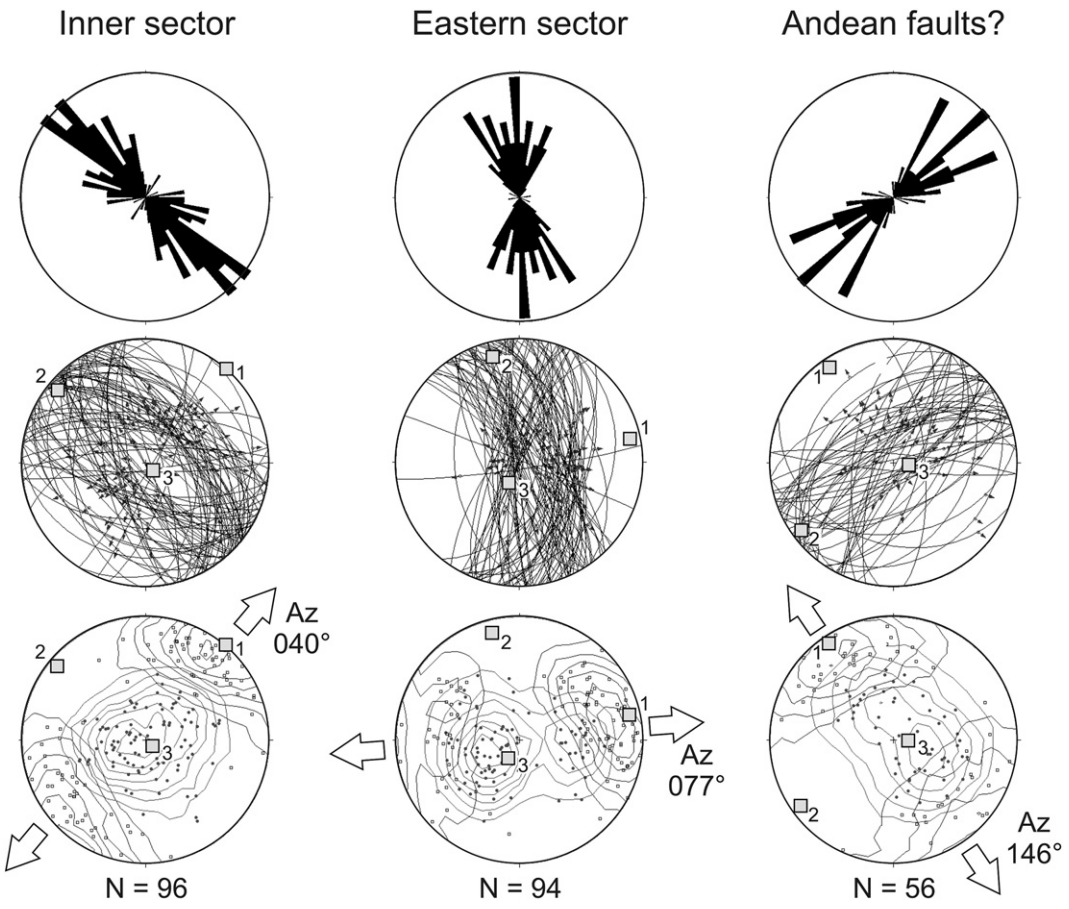

Fig. 10. Groups of third to fourth order faults, delimited according to their kinematic characteristics and geographic distribution. For each group, three kinds of diagrams are shown: 1) rose diagrams showing the trend distribution; 2) major circles representing the lower hemisphere projection of fault planes, with arrows showing the hanging-wall sense of movement; and 3) distribution of principal incremental shortening axes (P axes, black dots) and extension axes (T axes, unfilled squares). Grey squares represent the obtained axes of the strain ellipsoid ($\lambda 1$, $\lambda 2$ and $\lambda 3$) for each group of faults. N: number of data. Diagrams made using the FaultKinWin® and StereoWin® programs (Allmendinger, 2001, 2002).

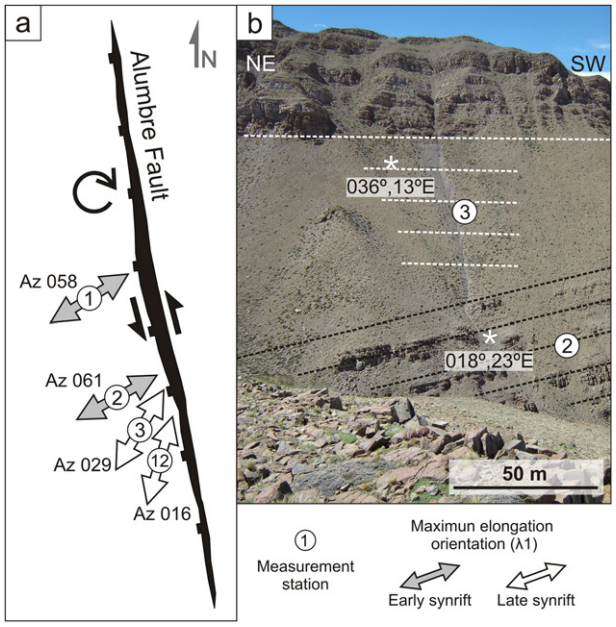

Fig. 11. a) Kinematic data from the hanging-wall of the Alumbre fault. Faults from early synrift deposits show a NE to ENE extension (stations 1 and 2), contrasting with a NNE extension obtained from late synrift sediments (stations 3 and 12). b) Angular unconformity between stations 2 and 3, coinciding with the change of the obtained $\lambda 1$ between these localities (see explanation in the text).

the northern Andean sector of the Neuquén basin (described in Giambiagi et al., 2009), most notably a) the NNW orientation of the extended area, with an eastern border controlled by the La Manga fault, b) the marine ingression registered in the depocenter western sector, where the only Triassic to Hettangian marine deposits described for the Neuquén basin crop out, and c) the marked lateral variations of the depositional environments during the synrift stage, as in the case of the Alumbre fault, which maintained a fixed coast line until the end of the Early Sinemurian period.

7. Discussion

7.1. Regional extension direction

There is no correlation between the variability of the obtained extension directions and the age of the synrift deposits where the measurements were made, so we cannot relate these differences to regional stress changes over time (Fig. 9). Moreover, the spatial variability of the obtained kinematic axes makes it difficult to interpret a uniform stress or strain field. Thus, the heterogeneity of our results seems to favor the hypothesis that the fault patterns reflect local deformations inside the Atuel depocenter. According to Gapais et al. (2000), the spatial variability of fault-slip data can be due to complications at the edges of fault blocks, or to complex kinematic conditions at regional limits.

However, we consider that we can make an approximation of the regional strain field by applying analytical models of

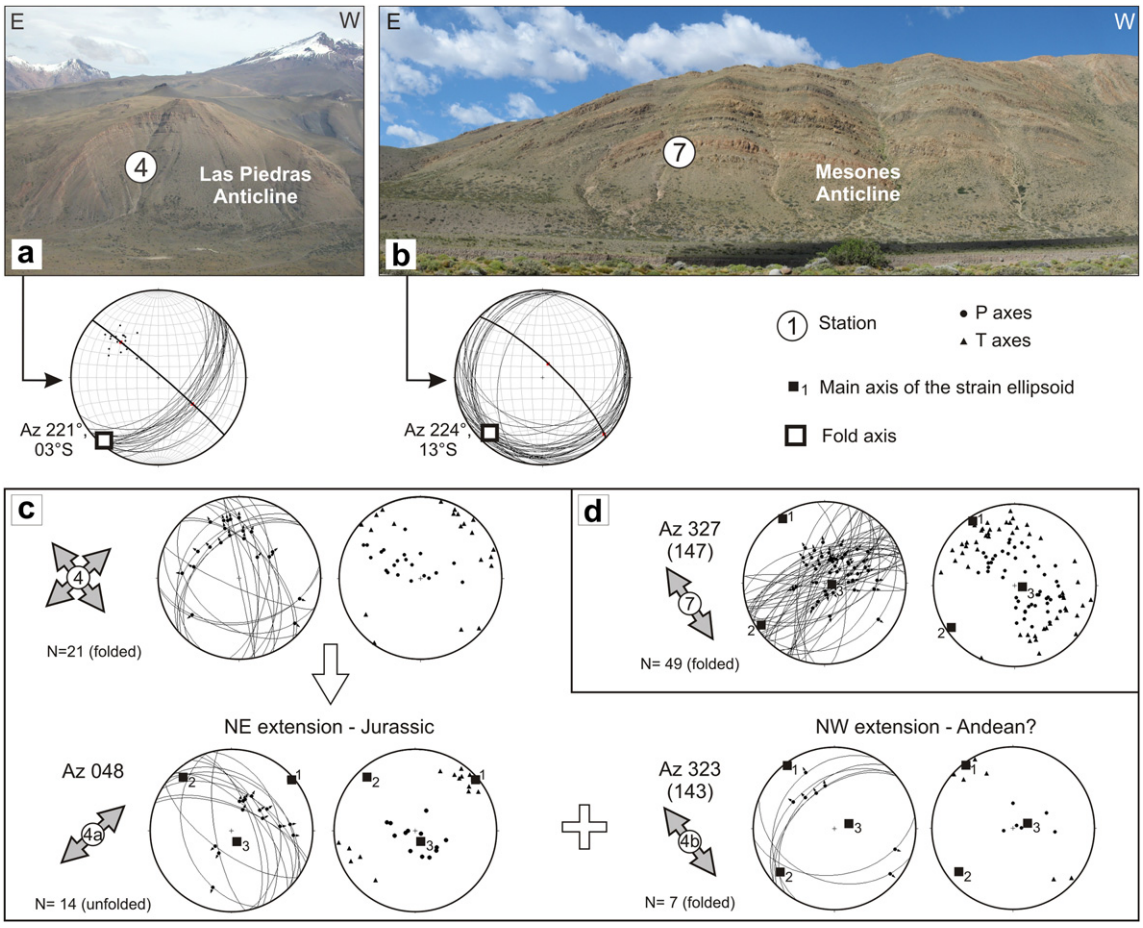

Fig. 12. a y b) NE-trending anticlines with fault-slip data indicating a NW-directed extension (stations 4 and 7; modified from Bechis et al., 2009). The diagrams below the photographs show the fold axis, calculated using attitude data from the fold limbs. c) Kinematic data from station 4, with a bimodal distribution of $\lambda 1$, indicating NE and NW extension directions (see explanation in the text). d) Kinematic data from station 7. Diagrams made using the FaultKinWin® and StereoWin® programs (Allmendinger, 2001, 2002).

transtensional settings. According to Tikoff and Teyssier (1994), and Teyssier et al. (1995), in a transtensional setting there is a refraction between the maximum instantaneous elongation ($s1^*$) inside the rift system, and the external divergence vector. For homogeneous non-partitioned transtension, they are related by the following equation (Teyssier et al., 1995):

$$\theta t = 1/2(90^\circ + \alpha)$$

where θt is the angle between the rift margin and the $s1^*$, and α is the angle between the rift margin and the external divergence vector (Fig. 13). The external divergence vector is generally not parallel to $s1^*$ ($\theta t \neq \alpha$), except in the case of orthogonal extension ($\alpha = 90^\circ$). For all other cases of oblique divergence, $s1^*$ is refracted relative to the external divergence direction.

For the Atuel depocenter, we take the extension directions obtained from the inversion of fault-slip data ($\lambda 1$) as an approximation of the maximum instantaneous elongation ($s1^*$). Using a N10°W orientation for the border of the rift system and the NE elongation direction we obtained from fault-slip data (mean $\lambda 1$ = Az 047°), we calculated an α angle of 24°. This α angle corresponds to a regional divergence oriented in a N14°E direction. Therefore, we estimate a NNE regional extension, with a probable refraction in a nearly NE direction for the internal oblique extension of the Atuel depocenter (Fig. 13).

7.2. Previous weakness control over the extensional strain of the Atuel depocenter

In oblique rift systems, the direction of extension is oblique to the trend of the basin, generally controlled by the presence of a lithospheric weakness or by a previous fabric of the upper-crustal basement (Tron and Brun, 1991; Holdsworth et al., 1997; Morley et al., 2004; Bellahsen et al, 2006). Lithospheric weaknesses can be related to ancient terrane sutures, previous orogenic belts, or areas thermally weakened by magmatic activity. These deep weakness zones generally control the location, areal extension and orientation of the rift systems. On the other hand, in areas where the previous fabric of the upper-crustal basement is weak and susceptible to reactivation, this fabric can be the main controlling factor over the orientation of the extensional system. In this case, reactivated structures can evolve as major normal faults during the early stages of the rift development, eventually controlling the general basin orientation (Morley et al., 2004; Bellahsen et al, 2006).

The basement of the Neuquén basin records a complex geological history, marked by allochtonous terrane accretions during the Early Paleozoic, followed by the Late Paleozoic San Rafael orogenic phase. The sutures and rheological contrasts between the accreted terrains, and the structures developed during the Paleozoic contractional stages have a general NW–NNW trend (Ramos, 1994; Chernicoff and Zappetini, 2003), and were interpreted by several authors as having controlled the development of rift systems from Early Triassic to

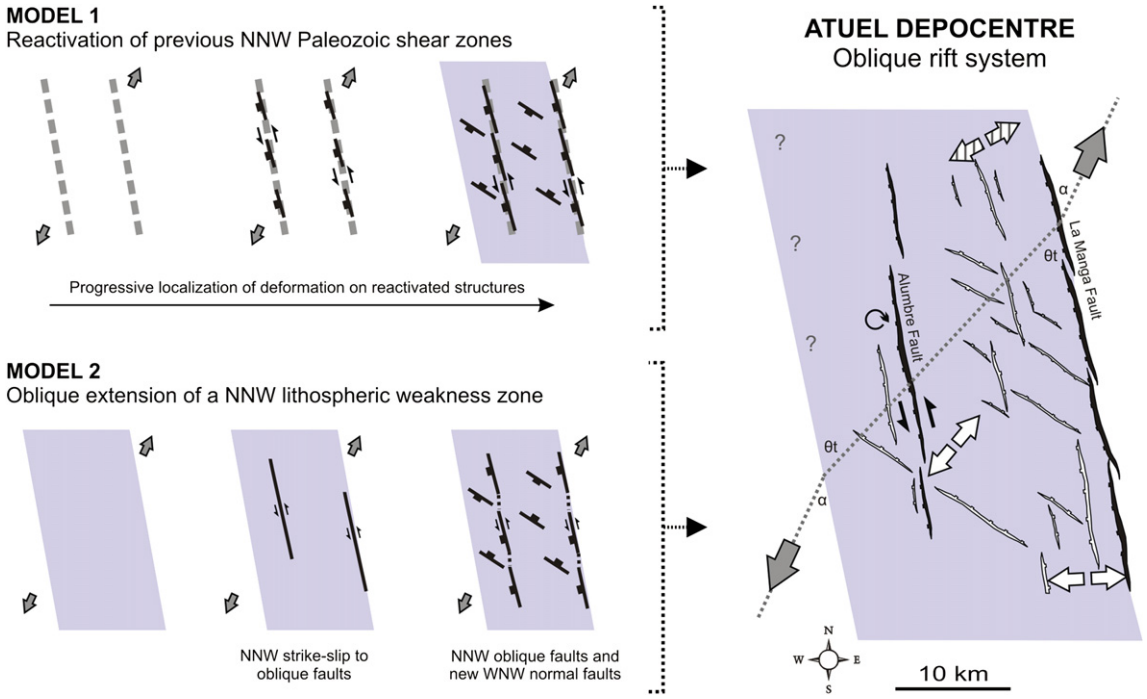

Fig. 13. Kinematic model of the Atuel depocenter as an oblique rift, and schematic representation of the two proposed models for the origin and evolution of this transtensional system (see explanation in the text). White arrows represent the local extension directions obtained in this contribution (Fig. 10), dashed arrows indicate the extension direction inferred by Giambiagi et al. (2005) for the northeastern sector, and the big grey arrows represent the inferred regional divergence. The dotted line shows a possible refraction of the strain due to the oblique extension inside the rifted area. α is the angle between the rift margin and the external divergence vector, and θt is the angle between the rift margin and the maximum instantaneous elongation inside the rift system.

Early Cretaceous times (Ramos, 1994; Mosquera and Ramos, 2006). In the case of the Atuel depocenter, we propose two possible options for the control of these pre-existing anisotropies over the development of the Atuel oblique rift system.

On the one hand, the NNW orientation of the main Alumbre and La Manga normal faults is similar to the trend of Upper Paleozoic shear zones, described by Kleiman and Japas (2009) in the nearby San Rafael block (Fig. 1). Taking into account this geometric similarity, these previous NNW-oriented shear zones may have been reactivated as normal-oblique faults under a regional NNE extension (Fig. 13, Model 1), as was previously proposed by Giambiagi et al. (2008a). A large slip focused on these reactivated structures might have finally controlled the NNW orientation of the Atuel depocenter, resulting in the development of an oblique rift system. In this case, the previous structures should correspond to a very weak discrete fabric of the upper crust, highly susceptible to reactivation (according to the classification of pre-existing anisotropies proposed by Morley et al., 2004).

On the other hand, the orientation of the Atuel sub-basin could have been controlled by a NNW-trending lithospheric weakness zone related to the suture between Chilenia and Cuyania terranes (Ramos, 1994; Chernicoff and Zappetini, 2003), obliquely oriented respect to a regional NNE extension (Fig. 13, Model 2). This case is analogue to physical models of oblique rifting, simulated by imposing a basal weakness zone obliquely oriented to the applied extension (Withjack and Jamison, 1986; Tron and Brun, 1991; Schreurs and Colleta, 1998; Bechis, 2009). According to the models, the Alumbre and La Manga major faults could have formed during the early stages of the rifting, in Late Triassic times, as long strike-slip to oblique-normal faults, sub-parallel to the rift border and oblique to the direction of extension (Schreurs and Colleta, 1998; Bechis, 2009). These NNW major faults could have acted as normal to oblique-normal faults during most of the later synrift, due to their favorable orientation for the accommodation of the extensional pure-shear component of the transtensional strain (Tikoff and Teyssier, 1994; Schreurs and Colleta, 1998; Bechis, 2009).

8. Conclusions

In this study, we identified four orders of faults for the extensional architecture of the Atuel depocenter, in the Neuquén basin northern sector. First to second order faults controlled major and minor variations of the depositional environments distribution, while third and fourth order faults accommodated local deformation in the hanging-wall of major faults. First order faults show a NNW trend, while second order faults show a NNW and WNW bimodal distribution. Third and fourth order faults have similar orientations, showing a higher dispersion of smaller faults.

We integrated data from these major and minor normal faults in a kinematic model for the Atuel depocenter. The general NNW depocenter orientation was controlled by a large slip localized in the identified first order faults (Alumbre and La Manga faults). The obliquity between the NNW extended area and the average NE internal extension direction calculated from fault-slip data (mean $\lambda 1 =$ Az 047°) enabled us to interpret that the depocenter evolved as an oblique rift system. Using kinematic data we characterized the Alumbre fault slip as left-lateral normal-oblique, while the La Manga fault could have had a similar slip during the early synrift, although its slip was predominantly normal during the late synrift stage.

The wide dispersion of the obtained kinematic axes did not enable us to infer the regional strain field, but we made an approximation by applying analytical models of transtensional settings. Using a N10°W orientation for the rift system border and the obtained NE internal elongation (mean $\lambda 1 =$ Az 047°), we calculated an α angle of 24°. This α angle corresponds to a regional divergence oriented in a N14°E direction. Therefore, we estimated

a NNE regional extension, with a probable refraction to a nearly NE direction for the internal oblique extension of the Atuel depocenter.

We proposed two options in order to evaluate the control of previous weakness zones as the possible cause for the development of the Atuel oblique rift system. In the first model, a weak discrete fabric affecting the basement of the basin, consisting of NNW-trending Upper Paleozoic shear zones, may have been reactivated as normal-oblique faults under a regional NNE extension. Another possible option is to consider an oblique extension of a previous NNW-oriented lithospheric weakness, related to a suture between terranes accreted during Early Paleozoic times, under a regional NNE divergence.

Acknowledgments

This work is based on part of Florencia Bechis's Ph.D. research. We wish to give special thanks to Alejandro Celli, Gabriela Da Poian, Diego Iaffa, Diego Kietzmann, José Mescua, Darío Orts, Sergio Orts, Marilin Peñalva, Julieta Suriano, Carla Terrizzano and Daniel Yagupsky for their invaluable help in the field. We also thank Drs. Susana Damborenea, Miguel Manceñido and Alberto Riccardi, who carried out the biostratigraphic studies at the Universidad Nacional de la Plata. The sub-surface information was kindly facilitated by Julián Fantín, Gonzalo Zamora Valcarce, Roberto Varade and Tomás Zapata, from Repsol-YPF. We are indebted to Melanie Berry for improving the English of the original manuscript. This research was funded by Agencia Nacional de Promoción Científica y Tecnológica (PICT 07-10942, PICT 38295), CONICET (PIP 5843), and Universidad de Buenos Aires (UBACYT 055). We thank Robert Holdsworth, Peter Cobbold and an anonymous reviewer for their valuable comments and suggestions.

References

Allmendinger, R.W., 2001. FaultKinWin Version 1.2.2. A Program for Analyzing Fault Slip Data for Windows™ Computers. http://www.geo.cornell.edu/geology/faculty/RWA/programs.html.

Allmendinger, R.W., 2002. StereoWin Version 1.2.0. http://www.geo.cornell.edu/geology/faculty/RWA/programs.html.

Angelier, J., 1984. Tectonic analysis of fault slip data sets. Journal of Geophysical Research 89 (B7), 5835–5848.

Baldauf, P., 1997. Timing of the Uplift of the Cordillera Principal, Mendoza Province, Argentina. Master Thesis. George Washington University, p. 356.

Bechis, F., 2009. Deformación transtensiva de la cuenca Neuquina: análisis a partir de ejemplos de campo y modelos análogos. Ph.D. Thesis. Facultad de Ciencias Exactas y Naturales, Universidad de Buenos Aires, p. 258.

Bechis, F., Giambiagi, L.B., Yagupsky, D.L., Cristallini, E.O., García, V.H., Mescua, J.F., 2008. Control of Mesozoic extensional structures on the Andean deformation in the northern Malargüe fold and thrust belt, Mendoza, Argentina. In: 7th International Symposium on Andean Geodynamics (ISAG), Nice, Extended Abstracts, pp. 71–74.

Bechis, F., Giambiagi, L.B., Lanés, S., García, V.H., Tunik, M., 2009. Evidencias de extensión oblicua en los depósitos de sinrift del sector norte de la cuenca neuquina. Revista de la Asociación Geológica Argentina 65 (2), 293–310.

Bellahsen, N., Fournier, M., d'Acremont, E., Leroy, S., Daniel, J.M., 2006. Fault reactivation and rift localization: Northeastern Gulf of Aden margin. Tectonics 25, TC1007. doi:10.1029/2004TC001626, p. 14.

Chernicoff, C.J., Zappetini, E.O., 2003. Delimitación de los terrenos tectono-estratigráficos de la región centro-austral Argentina: evidencias aeromagnéticas. Revista Geológica de Chile 30 (2), 299–316.

Cobbold, P.R., Rosello, E.A., 2003. Aptian to recent contractional deformation, foothills of the Neuquén basin, Argentina. Marine and Petroleum Geology 20 (5), 429–443.

Combina, A.M., Nullo, F., 2000. La Formación Loma Fiera (Mioceno superior) y su relación con el volcanismo y el tectonismo neógeno, Mendoza. Revista de la Asociación Geológica Argentina 55 (3), 201–210.

Dimieri, L., Fortunatti, N., Nullo, F., 2005. Estructura duplex plegada en el frente montañoso de la Cordillera Principal, Río Atuel, provincia de Mendoza. Revista de la Asociación Geológica Argentina 60 (4), 644–650.

Fortunatti, N., Dimieri, L., 2006. Tectónica del valle del río Atuel al pie del Cerro Sosneado, Provincia de Mendoza. In: Asociación Geológica Argentina, Publicación Especial, Serie D, No 9, pp. 56–61.

Franzese, J.R., Spalletti, L.A., 2001. Late Triassic – early Jurassic continental extension in southwestern Gondwana: tectonic segmentation and pre-break-up rifting. Journal of South American Earth Sciences 14, 257–270.

Gapais, D., Cobbold, P.R., Bourgeois, O., Rouby, D., de Urreiztieta, M., 2000. Tectonic significance of fault-slip data. Journal of Structural Geology 22, 881–888.

Giambiagi, L.B., Suriano, J., Mescua, J., 2005. Extensión multiepisódica durante el Jurásico Temprano en el depocentro Atuel de la cuenca Neuquina. Revista de la Asociación Geológica Argentina 60 (3), 524–534.

Giambiagi, L.B., Bechis, F., Lanés, S., Tunik, M., García, V., Suriano, J., Mescua, J., 2008a. Formación y evolución triásico-jurásica del depocentro Atuel, cuenca Neuquina, provincia de Mendoza, Argentina. Revista de la Asociación Geológica Argentina 63 (4), 520–533.

Giambiagi, L.B., Bechis, F., García, V.H., Clark, A., 2008b. Temporal and spatial relationships of thick- and thin-skinned deformation in the Malargüe fold and thrust belt, Southern Central Andes. Tectonophysics 459 (1–4), 123–139.

Giambiagi, L.B., Tunik, M., Barredo, S., Bechis, F., Ghiglione, M., Alvarez, P., Drosina, M., 2009. Cinemática de apertura del sector norte de la cuenca neuquina. Revista de la Asociación Geológica Argentina 65 (2), 278–292.

Gulisano, C.A., Gutiérrez Pleimling, A.R., 1994. The Jurassic of the Neuquén Basin: b) MendozaProvince. Guía de Campo. In: Asociación Geológica Argentina, Publicación Especial, Serie E, No 3, p. 103.

Hardy, S., McClay, K., 1999. Kinematic modeling of extensional fault propagation folding. Journal of Structural Geology 21, 695–702.

Holdsworth, R.E., Butler, C.A., Roberts, A.M., 1997. The recognition of reactivation during continental deformation. Journal of the Geological Society, London 154, 73–78.

Iglesia Llanos, M.P., Riccardi, A.C., Singer, S.E., 2006. Palaeomagnetic study of Lower Jurassic marine strata from the Neuquén Basin, Argentina: a new Jurassic apparent polar wander path for South America. Earth and Planetary Science Letters 252, 379–397.

Kleiman, L.E., Japas, M.S., 2009. The Choiyoi volcanic province at 34°S-36°S (San Rafael, Mendoza, Argentina): implications for the late Palaeozoic evolution of the southwestern margin of Gondwana. Tectonophysics 473 (3–4), 283–299.

Kozlowski, E., 1984. Interpretación estructural de la Cuchilla de la Tristeza, provincia de Mendoza. 9 Congreso Geológico Argentino, San Carlos de Bariloche, Actas. 2, 381–395.

Kozlowski, E., Manceda, R., Ramos, V.A., 1993. Estructura. In: Ramos, V.A. (Ed.), Geología y recursos naturales de Mendoza. 12° Congreso Geológico Argentino y 2° Congreso de Exploración de Hidrocarburos. Relatorio, Mendoza, pp. 235–256.

Lanés, S., 2002. Paleoambientes y Paleogeografía de la primera transgresión en Cuenca Neuquina, Sur de Mendoza. Ph.D. Thesis. Facultad de Ciencias Exactas y Naturales, Universidad de Buenos Aires, p. 403.

Lanés, S., 2005. Late Triassic to early Jurassic sedimentation in northern Neuquén basin, Argentina: Tectonosedimentary evolution of the first transgression. Geologica Acta 3 (2), 81–106.

Lanés, S., Giambiagi, L.B., Bechis, F., Tunik, M., 2008. Late Triassic – early Jurassic successions of the Atuel depocenter: sequence stratigraphy and tectonic controls. Revista de la Asociación Geológica Argentina 63 (4), 534–548.

Legarreta, L., Gulisano, C.A., Uliana, M.A., 1993. Las secuencias sedimentarias jurásico-cretácicas. In: Ramos, V.A. (Ed.), Geología y Recursos Naturales de Mendoza, 12° Congreso Geológico Argentino y 2° Congreso de Exploración de Hidrocarburos. Relatorio, Mendoza, pp. 87–114.

Legarreta, L., Uliana, M.A., 1996. The Jurassic succesion in west-central Argentina: stratal patterns, sequences and paleogeographic evolution. Palaegeography, Palaeoclimatology and Palaeoecology 120, 303–330.

Llambías, E.J., Kleinman, L.E., Salvarradi, J.A., 1993. El magmatismo Gondwánico. In: Ramos, V.A. (Ed.), Geología y Recursos Naturales de Mendoza. 12° Congreso Geológico Argentino y 2° Congreso de Exploración de Hidrocarburos. Relatorio, Mendoza, pp. 53–64.

Iglesia Llanos, M.P., 2008. Paleogeografía de América del Sur durante el Jurásico. Revista de la Asociación Geológica Argentina 63 (4), 498–511.

Manceda, R., Figueroa, D., 1995. Inversion of the Mesozoic Neuquén rift in the Malargüe fold-thrust belt, Mendoza, Argentina. In: Tankard, A.J., Suárez, R., Welsink, H.J. (Eds.), Petroleum Basins of South America. American Association of Petroleum Geologists, Memoir 62, pp. 369–382.

Marrett, R., Allmendinger, R.W., 1990. Kinematic analysis of fault-slip data. Journal of Structural Geology 12 (8), 973–986.

Morley, C.K., Haranya, C., Phoosongsee, W., Pongwapee, S., Kornsawan, A., Wonganan, N., 2004. Activation of rift oblique and rift parallel pre-existing fabrics during extension and their effect on deformation style: examples from the rifts of Thailand. Journal of Structural Geology 26, 1803–1829.

Mosquera, A., Ramos, V.A., 2006. Intraplate deformation in the Neuquén embayment. In: Kay, S.M., Ramos, V.A. (Eds.), Evolution of an Andean Margin: a Tectonic and Magmatic View from the Andes to the Neuquén Basin (35°–39°S lat). Geological Society of America, Special Paper, 407, pp. 97–123.

Nullo, F., Stephens, G., Otamendi, J., Baldauf, P., 2002. El volcanismo del Terciario superior del sur de Mendoza. Revista de la Asociación Geológica Argentina 57 (2), 119–132.

Petit, J.P., 1987. Criteria for the sense of movement on fault surfaces in brittle rocks. Journal of Structural Geology 9 (5–6), 597–608.

Ramos, V.A., 1994. Terranes of southern Gondwanaland and their control in the Andean structure (30°–33°S latitude). In: Reutter, K.J., Scheuber, E., Wigger, P. (Eds.), Tectonics of the Southern Central Andes. Springer, Berlin, pp. 249–261.

Ramos, V.A., 2010. The tectonic regime along the Andes: present-day and Mesozoic regimes. Geological Journal 45, 2–25.

Reijenstein, C., 1967. Estratigrafía y tectónica de la zona al Norte del río Atuel, entre los arroyos Blanco y Malo, provincia de Mendoza. Licenciatura Thesis. Facultad de Ciencias Exactas y Naturales, Universidad de Buenos Aires, p. 67.
Riccardi, A.C., Damborenea, S., Manceñido, M.O., Ballent, S.C., 1991. Hettangian and Sinemurian (Lower Jurassic) biostratigraphy of Argentina. Journal of South American Earth Sciences 4 (3), 159–170.
Riccardi, A.C., Damborenea, S.E., Manceñido, M.O., Scasso, S., Lanés, S., Iglesia Llanos, M.P., 1997. Primer registro de Triásico marino fosilífero de la Argentina. Revista de la Asociación Geológica Argentina 52 (2), 228–234.
Schreurs, G., Colleta, B., 1998. Analogue modelling of faulting in zones of continental transpression and transtension. In: Holdsworth, R.E., Stracnan, R.A., Dewey, J.E. (Eds.), Continental Transpressional and Transtensional Tectonics. Geological Society, London, Special Publications, 135, pp. 59–79.
Somoza, R., Zaffarana, C.B., 2008. Mid-Cretaceous polar standstill of South America, motion of the Atlantic hotspots and the birth of the Andean cordillera. Earth and Planetary Science Letters 271, 267–277.
Spalletti, L.A., Morel, E.M., Franzese, J.R., Artabe, A.E., Ganuza, D., Zúñiga, A., 2007. Contribución al conocimiento sedimentológico y paleobotánico de la Formación El Freno (Jurásico Temprano) en el valle superior del río Atuel, Mendoza, Argentina. Ameghiniana 44 (2), 367–386.
Sruoga, P., Etcheverría, M., Folguera, A., Repol, D., Zanettini, J.C., 2005. Hoja Geológica 3569-I Volcán Maipo, 290. Servicio Geológico y Minero Argentino, Boletín, p. 116.
Teyssier, C., Tikoff, B., Markley, M., 1995. Oblique plate motion and continental tectonics. Geology 23 (5), 447–450.
Tikoff, B., Teyssier, C., 1994. Strain modelling of displacement-field partitioning in transpressional orogens. Journal of Structural Geology 16 (11), 1575–1588.
Tron, V., Brun, J.P., 1991. Experiments on oblique rifting in brittle-ductile systems. Tectonophysics 188, 71–84.
Tunik, M., Lanés, S., Bechis, F., Giambiagi, L.B., 2008. Analisis petrográfico preliminar de las areniscas jurásicas tempranas en el depocentro Atuel de la cuenca Neuquina. Revista de la Asociación Geológica Argentina 63 (4), 714–727.
Turienzo, M., Dimieri, L., 2005. Geometric and kinematic model for basement-involved backthrusting at Diamante River, southern Andes, Mendoza province, Argentina. Journal of South American Earth Sciences 19, 111–125.
Twiss, R.J., Unruh, J.R., 1998. Analysis of fault slip inversions: do they constrain stress or strain rate? Journal of Geophysical Research 103 (B6), 12205–12222.
Uliana, M.A., Biddle, K.T., Cerdán, J., 1989. Mesozoic extension and the formation of Argentine sedimentary basins. In: Tankard, A., Balkwill, H.R. (Eds.), Extensional Tectonics and Stratigraphy of the North Atlantic Margins. American Association of Petroleum Geologists, Memoir 46, pp. 599–614.
Vergani, G.D., Tankard, J., Belotti, J., Welsink, J., 1995. Tectonic evolution and paleogeography of the Neuquén Basin, Argentina. In: Tankard, A.J., Suárez, R., Welsink, H.J. (Eds.), Petroleum Basins of South America. American Association of Petroleum Geologists, Memoir 62, pp. 383–402.
Volkheimer, W., 1978. Descripción Geológica de la Hoja 27b, Cerro Sosneado, provincia de Mendoza, 151. Servicio Geológico Nacional, Boletín N, p. 83.
Withjack, M.O., Jamison, W.R., 1986. Deformation produced by oblique rifting. Tectonophysics 126, 99–124.
Yrigoyen, M.R., 1993. Los depósitos sinorogénicos terciarios. In: Ramos, V.A. (Ed.), Geología y Recursos Naturales de Mendoza. 12° Congreso Geológico Argentino y 2° Congreso de Exploración de Hidrocarburos. Relatorio, pp. 123–148.
Zamora Valcarce, G., Zapata, T.R., del Pino, D., Ansa, A., 2006. Structural evolution and magmatic characteristics of the Agrio fold-and-thrust belt. In: Kay, S.M., Ramos, V.A. (Eds.), Evolution of an Andean Margin: a Tectonic and Magmatic View from the Andes to the NeuquénBasin (35°-39°S lat). Geological Society of America, Special Paper, 407, pp. 125–145.